

Soft Matter

Accepted Manuscript



This is an *Accepted Manuscript*, which has been through the Royal Society of Chemistry peer review process and has been accepted for publication.

Accepted Manuscripts are published online shortly after acceptance, before technical editing, formatting and proof reading. Using this free service, authors can make their results available to the community, in citable form, before we publish the edited article. We will replace this *Accepted Manuscript* with the edited and formatted *Advance Article* as soon as it is available.

You can find more information about *Accepted Manuscripts* in the [Information for Authors](#).

Please note that technical editing may introduce minor changes to the text and/or graphics, which may alter content. The journal's standard [Terms & Conditions](#) and the [Ethical guidelines](#) still apply. In no event shall the Royal Society of Chemistry be held responsible for any errors or omissions in this *Accepted Manuscript* or any consequences arising from the use of any information it contains.

Phase Segregation in Bio-Inspired Multi-Component Vesicles Encompassing Double Tail Phospholipid Species

Fikret Aydin, Paul Ludford and Meenakshi Dutt**

Department of Chemical Engineering, Rutgers The State University of New Jersey, Piscataway, NJ 08854

ABSTRACT

Our aim is to investigate the phase segregation and structure of multi-component bio-inspired phospholipid vesicles via Dissipative Particle Dynamics. The chemical distinction in the phospholipid species arise due to different head and tail group moieties, and molecular stiffness of the hydrocarbon tails. The individual amphiphilic phospholipid molecular species are represented by a hydrophilic head group and two hydrophobic tails. The distinct chemical nature of the moieties is modeled effectively via soft repulsive interaction parameters, and the molecular rigidity is tuned via suitable three-body potential constants. We demonstrate the formation of a stable hybrid vesicle through the self-assembly of the amphiphilic phospholipid molecules in the presence of a hydrophilic solvent. We investigate and characterize the phase segregation and structure of the binary vesicles for different phospholipid mixtures. Our results demonstrate macroscopic phase separation for phospholipid mixtures composed of species with different hydrocarbon tail groups. We also investigate the relation between the phase segregation and thermodynamic variables such as interfacial line tension and surface tension, and obtain correspondence between existing theory and experiments, and our simulation results. We report variations in the molecular chain stiffness to have negligible contributions to the phase segregation in the mixed bilayer, and to demonstrate shape transformations of the hybrid vesicle. Our results can be used to design novel bio-inspired hybrid vehicles for potential applications in biomedicine, sensing, imaging and sustainability.

Keywords: vesicles, bilayers, phospholipids, coarsening dynamics, dissipative particle dynamics

** corresponding author: meenakshi.dutt@rutgers.edu

INTRODUCTION

Biological cell membranes are dynamic, responsive multi-component soft materials which separate and protect the cellular contents from the external environment, and participate in vital functions, such as intracellular and extracellular traffic, sensing and cell signaling.¹⁻⁴ These membranes are composed of a variety of amphiphatic molecules which can self-organize to modulate the membrane tension and thereby, its mechanical properties to facilitate various physiological processes, or promote binding or catalytic events at the membrane interface.^{2,3,5} Earlier studies² have shown phospholipid molecules to be the primary component of cell membranes; these amphiphilic entities have a hydrophilic head group and two hydrocarbon tail chains. The head and tail groups of the phospholipid species can have distinct chemistries which endows a characteristic molecular geometry^{6,7} and transition temperature⁸⁻¹⁰, and drives the self-organization of the various species into domains or rafts.^{4,11-24} Investigations have shown domain and raft formation in cell membranes to be critical for vital physiological functions such as cell signaling and signal transduction.^{2,25} Therapeutic approaches based upon targeting these functions will require a fundamental understanding of the processes driving the formation of domain and rafts in a cell membrane. We are interested in investigating the role of the distinction in the head and tail group chemistry of phospholipids on the phase segregation in bio-inspired cells.

Macroscopic sized domains have been shown to form in ternary mixtures composed of a lipid with low melting temperature, a lipid with high melting temperature and cholesterol.^{11,16,26,27} The relative concentrations of the lipids and the temperature determine the area fraction of each phase. For temperatures corresponding to a two-phase region: the early stages of the coarsening dynamics is accompanied by the nucleation of small domains due to the lateral diffusion and collision between the lipid molecules followed by their coalescence, or the Ostwald ripening mechanism.¹⁶ At latter times, the growth of the domains occurs via their diffusion, collision and coalescence, with the kinetics determined by the membrane and the bulk fluid.^{16,28} Experimental^{11,16,26,27} and numerical^{4,14,15,17,18,23,28-31} studies on phase segregation in multi-component bilayers have measured the growth kinetics and morphology of the domains. Computational studies have adopted implicit solvent models to investigate coarsening dynamics via Monte Carlo³² and Molecular Dynamics²³ techniques. Other studies have used Molecular Dynamics-based approaches which reproduce the hydrodynamic behavior in multi-component lipid vesicles.^{4,14,15,29,30} In addition, studies using continuum approaches^{17,18,28} have also explored the phase separation process and associated kinetics in multi-component membranes. For membranes with equal concentrations of the two lipids and at a temperature below the critical miscibility value, the domain boundaries fluctuate with a correlation length which, along with the hydrodynamic radius, will determine the coarsening dynamics.^{13,26,27}

The existing particle-based numerical studies on the coarsening dynamics in multi-component bilayers have modeled the lipid molecules with a single hydrocarbon chain.^{4,14,15,23,29} Investigations on binary vesicles composed of two-tail lipids of different chain length have explored the effect of the relative concentration of one of the lipid species on the mechanical properties of the vesicles.³⁰ We have focused our investigations on a bilayer vesicle composed of two types of phospholipid molecules (each species has two hydrocarbon tails) which are the major component of biological cell membranes. Studies on multi-component vesicles have identified four key length scales which determine the phase segregation process: the

hydrodynamic diameter, the domain size, the correlation length for domains in the vicinity of a critical miscibility limit and the vesicle diameter.¹⁶ We consider these key length scales by adopting a mesoscopic particle-based computational approach entitled Dissipative Particle Dynamics (DPD)^{4,14,15,29,30,33-45} which simultaneously resolves both the molecular and continuum scales. Numerical studies of the mesoscopic dynamical, structural and morphological properties of fluid bilayer membranes^{1,43} via the DPD approach have demonstrated good agreement with experimental results. In addition, the DPD method has been used to investigate the dynamical and morphological properties of block co-polymers,^{46,47} dense colloidal suspensions,⁴⁸ polymers in dilute solution or in a melt⁴⁹ and chains in microfluidic channels via the use of coarse-grained models.^{50,51} Similar approaches have been utilized to examine the equilibrated structures of self-assembling lipid systems⁵² and phase separation in binary lipid vesicles.^{4,14,15,29} The DPD simulation technique has also been used to demonstrate phase transitions in lipid bilayer membranes through the use of coarse-grained models of the lipid molecules.⁵³⁻⁵⁶ We would like to note that coarse-grained models have also been used along with other techniques such as Molecular Dynamics (MD) to demonstrate dynamic properties in polyethylene melts⁵⁷ and phase transitions in lipid bilayers.⁵⁸⁻⁶⁰

In this paper, we use the DPD technique to investigate the role of chemical dissimilarity in the head and tail groups of the lipid species on the phase segregation and structural properties of binary vesicles. We model the effective distinction in the chemical nature of the lipid head and tail groups through the soft repulsive interaction parameters. To identify the effect of the molecular stiffness on the phase segregation process and the vesicle shape, we vary the molecular chain stiffness of one type of lipid. Our investigations can be potentially used to understand the fundamental processes underlying cellular physiological functions, such as domain or raft formation⁶¹⁻⁶³ or shape transformations in red blood cells.^{38,64,65}

METHODOLOGY

DPD is a mesoscopic MD-based simulation technique that uses soft-sphere coarse-grained (CG) models to capture both the molecular details of the system components and their supramolecular organization while simultaneously resolving the hydrodynamics of the system over extended time scales.^{33,41-45} In order to capture the dynamics of the soft spheres, the DPD technique integrates Newton's equation of motion via the use of similar numerical integrators used in other deterministic particle-based simulation methods.^{33,66} The force acting on a soft sphere i due to its interactions with a neighboring soft sphere j ($j \neq i$) has three components: a conservative force, a dissipative force and a random force, which operate within a certain cut-off distance r_c from the reference particle i . These forces are pairwise additive and yield the total force acting on particle i , which is given by $\mathbf{F}_i = \sum_{j \neq i} \mathbf{F}_{c,ij} + \mathbf{F}_{d,ij} + \mathbf{F}_{r,ij}$. The soft spheres interact via

a soft-repulsive force ($\mathbf{F}_{c,ij} = a_{ij}(1 - \frac{r_{ij}}{r_c})\hat{\mathbf{r}}_{ij}$, for $r_{ij} < r_c$ and $\mathbf{F}_{c,ij} = 0$, for $r_{ij} \geq r_c$), a dissipative force ($\mathbf{F}_{d,ij} = -\gamma\omega^d(r_{ij})(\hat{\mathbf{r}}_{ij} \cdot \mathbf{v}_{ij})\hat{\mathbf{r}}_{ij}$) and a random force ($\mathbf{F}_{r,ij} = -\sigma\omega^r(r_{ij})\theta_{ij}\hat{\mathbf{r}}_{ij}$), where $\omega^d(r) = [w^r(r)]^2 = (1-r)^2$ (for $r < 1$), $\omega^d(r) = [w^r(r)]^2 = 0$ (for $r \geq 1$) and $\sigma^2 = 2\gamma k_B T$. a_{ij} is the maximum repulsion between spheres i and j , $\mathbf{v}_{ij} = \mathbf{v}_i - \mathbf{v}_j$ is the relative velocity of the two spheres, $\mathbf{r}_{ij} = \mathbf{r}_i - \mathbf{r}_j$, $r_{ij} = |\mathbf{r}_i - \mathbf{r}_j|$, $\hat{\mathbf{r}}_{ij} = \mathbf{r}_{ij}/r_{ij}$, $r = r_{ij}/r_c$, γ is viscosity related parameter used in the

simulations, σ is the noise amplitude, $\theta_{ij}(t)$ is a randomly fluctuating variable from Gaussian statistics, ω^d and ω^r are the separation dependent weight functions which become zero at distances greater than or equal to the cutoff distance r_c . Each force conserves linear and angular momentum. Since the local momentum is conserved by all of these three forces, even the small systems exhibit hydrodynamic behavior.³³ The constraints imposed on the random and dissipative forces by certain relations ensure that the statistical mechanics of the system conforms to the canonical ensemble.^{33,66} The relation between the pair repulsion parameter a_{ij} and the Flory interaction parameter χ for a bead number density $\rho = 3r_c^{-3}$ is given by $\chi = (0.286 \pm 0.002)(a_{ij} - a_{ii})$.³³

As shown in Fig. 1 (a), the individual lipid molecules are represented by bead-spring models, and are modeled by a head group comprised of three hydrophilic beads and two hydrocarbon tails represented by three hydrophobic beads each. Two consecutive beads in a chain are connected via a bond that is described by the harmonic spring potential $E_{bond} = K_{bond}((r-b)/r_c)^2$, where K_{bond} is the bond constant and b is the equilibrium bond length. The constants, K_{bond} and b are assigned to the values of 64ϵ and $0.5r_c$, respectively.^{34,41-45} The three-body stiffness potential along the lipid tails has the form $E_{angle} = K_{angle}(1 + \cos \theta)$ where θ is the angle formed by three adjacent beads. The coefficient K_{angle} is set to be 20ϵ in our simulations. This stiffness term increases the stability and bending rigidity of the bilayers.⁴⁴

In this paper, we investigate the role of the effective distinction between two amphiphilic lipid species on the coarsening dynamics in a binary lipid bilayer vesicle, as shown in Fig. 1 (b). The dissimilarity in the amphiphilic lipid species can arise due to differences in the chemistry of the head or tail groups, which can be modeled effectively through a soft repulsive interaction parameter a_{ij} . Differences in the tail groups can also arise due to molecular chain stiffness that is captured in our model by suitably tuning the hydrophobic tail stiffness parameter K_{angle} .

The soft repulsive pair potential parameters for the lipid molecule head and tail beads were selected to capture its amphiphilic nature. The interaction parameters between the like components, a_{ij} , are based on the property of water.³³ The repulsion parameter between two beads of the same type is set at $a_{ii} = 25$ (measured in units of $k_B T / r_c$) which is based upon the compressibility of water at room temperature³³ for a bead density of $\rho = 3r_c^{-3}$. The soft repulsive interaction parameter a_{ij} between hydrophobic and hydrophilic beads is set at $a_{ij} = 100 k_B T / r_c$, and is determined by using the Flory-Huggins interaction parameters, χ , as $a_{ij} = a_{ii} + 3.496 \chi$ ³³, for $\rho = 3r_c^{-3}$.

The soft repulsive interaction parameters between the head (h), tail (t) beads of lipid types 1 and 2, and the solvent (s) beads are assigned the following values (in units of $k_B T / r_c$): $a_{ss} = 25$, $a_{h1h1} = 25$, $a_{t1t1} = 25$, $a_{h2h2} = 25$, $a_{t2t2} = 25$, $a_{h1t1} = 100$, $a_{h1s} = 25$, $a_{t1s} = 100$, $a_{h2t2} = 100$, $a_{h2s} = 25$, $a_{t2s} = 100$, $a_{h1t2} = 100$ and $a_{h2t1} = 100$. The values of the inter-lipid species head-head a_{h1h2} and tail-tail a_{t1t2} soft repulsive interaction parameters will span values ranging from 26 to 50, to

mimic mixtures of lipid species with different head or tail group properties. The soft repulsive interaction parameters are summarized in Table 1. These parameters are selected to model the effective distinct chemistry of the molecular species, thereby capturing the differences in the melting temperature of the individual species.^{4,14,15,23,29-31,67,68} This approach enables us to develop a simple representation of mixtures composed of lipids with two hydrocarbon tails.

In our simulations, the respective characteristic length scale and energy scale are r_c and $k_B T$. As a result, our characteristic time scale can be described as $\tau = \sqrt{mr_c^2 / k_B T}$. Finally, $\sigma = 3$ and $\Delta t = 0.02\tau$ are used in the simulations along with the total bead number density of $\rho = 3r_c^{-3}$ and a dimensionless value of $r_c = 1$.³⁴ The mass of all the beads is set to unity.^{1,3,30,33,34,41-45,53-56}

We used a constant volume simulation box of dimensions $40 \times 40 \times 40 r_c^3$ with the periodic boundary conditions in all three directions. In our simulations, we have 1178 lipid molecules, or 5.6% bead concentration of amphiphilic species, with 10602 head and tail beads. The total number of beads in the system (including solvent molecules) is 192,000.

We draw a correspondence between our model and physical systems via the experimental properties of biological lipid bilayers. We obtain the characteristic length scale for our model through the comparison of experimental measurements of the interfacial area per lipid of a DPPC bilayer with similar measurements from our simulations. Experimental measurements of the area per lipid of DPPC bilayers were found to be 64 \AA^2 at $50 \text{ }^\circ\text{C}$.⁶⁹ To compute the average area per lipid, the vesicle is divided into 128 rectangular patches with an average area of $10.5 r_c^2$ so that each patch can be treated as a bilayer membrane. The average area per lipid for the vesicle bilayer is computed by summing the areas of all the patches, and averaging over the total number of lipid molecules in all the patches. Using the value for the area per lipid ($1.12 r_c^2$) computed for a stable self-assembled single component lipid vesicle, the length scale for our model is $r_c = 0.76 \text{ nm}$.

The time scale τ was calculated to be 6.0 ns by comparing the experimental measurement of the diffusion coefficient of dipalmitoylphosphatidylcholine (DPPC) bilayer, which is given by $5 \times 10^{-12} \text{ m}^2/\text{s}$,³⁴ with that obtained from the simulations. The diffusion coefficient of the lipid molecule in the simulations can be found by tracking the mean squared displacements of 10 lipid molecules in a vesicle bilayer. We use the relation $\frac{\langle r^2(t) \rangle}{\alpha} = 2dD$ to relate the diffusion coefficient D to the mean square displacement of a particle in a time interval t .⁷⁰ The variable d is the dimensionality of the system that is given to be 3 for our system. We calculate the diffusion coefficient D to be $0.052 r_c^2 / \tau$, using the slope of the time evolution of the mean square displacement. Using a temperature of $50 \text{ }^\circ\text{C}$, the energy scale is calculated to be $\epsilon = k_B T = 4.5 \times 10^{-21} \text{ J}$.

RESULTS AND DISCUSSIONS

We begin by verifying the suitability of the soft repulsive interaction parameters for generating stable binary lipid vesicles. Via self-assembly of amphiphilic phospholipids in a hydrophilic solvent, we generate a binary lipid vesicle.⁷¹ We randomly disperse two types of amphiphilic

lipid molecules and hydrophilic solvent beads in a $30 r_c \times 30 r_c \times 30 r_c$ simulation box composed of 5.6 % bead concentration of amphiphilic species, or 504 lipid molecules.^{42,52} To enable the formation of a stable mixed vesicle, we tune the pair interaction potentials to effectively treat both types of lipid molecules as a single specie. The unfavorable enthalpic interactions between the hydrophilic and hydrophobic components drives the system to minimize its free energy through the self-assembly of the lipid molecules to form a lipid bilayer vesicle.⁷¹ In this paper, we will use similar soft repulsive interaction parameters to investigate the role of different head and tail group moieties on the coarsening dynamics in larger binary lipid vesicles.

We use a stable pre-assembled mixed vesicle composed of two chemically dissimilar amphiphilic lipid molecules in a $40 r_c \times 40 r_c \times 40 r_c$ simulation box composed of 1178 lipid molecules with 589 molecules of specie 1 and the remaining 589 molecules belonging to specie 2. We adopted an analogous protocol detailed earlier to generate a mixed binary vesicle by treating both the lipid types as a single specie, as shown in Fig. 1 (b). We investigate the self-organization of the lipid species for values of the head-head and tail-tail interaction parameters, respectively a_{h1h2} and a_{t1t2} , ranging from 26 to 50 for a time interval of 10000 τ .

The coarsening dynamics for bilayers composed of lipid species with chemically distinct head groups (and identical tail groups, for example 1-Palmitoyl-2-oleoylphosphatidylcholine and 1-Palmitoyl-2-oleoyl-sn-glycero-3-phosphoethanolamine) is shown in Fig. 2. The interfacial tension arising from the unfavorable enthalpic interactions between the distinct head groups drives chemically identical lipids to organize into small domains or clusters, via their diffusion and collision in the vesicle bilayer. Therefore, the self-organization among the lipid species is limited by the lateral diffusion of the different lipid species. Our calculations show the unfavorable enthalpic interactions between the head groups of the distinct lipid species to be small compared to the favorable enthalpic interactions between the hydrocarbon tail groups.

For bilayers composed of lipid species with dissimilar tail groups (and identical head groups, for example 1,2-distearoyl-sn-glycero-3-phosphocholine and 1,2-Dipalmitoyl-sn-glycero-3-phosphocholine), the highly unfavorable enthalpic interactions between the hydrocarbon groups results in a large interfacial energy. The system minimizes its free energy via the interfacial energy through the self-organization of the two molecular species into small domains in the bilayer, mediated by the diffusion and collision of the lipid molecules. For sufficiently high interfacial tension between the distinct lipid species, as the domains grow in the system the coarsening dynamics progresses through the diffusion and collision of the domains, or the evaporation-condensation mechanism. In the latter, individual lipid molecules are observed to evaporate from the boundaries of small domains and condense into the larger domains.^{4,14,15,22,27} We observe these processes for binary vesicles comprising of lipid species with greater dissimilarity between the tail groups.

The coarsening dynamics of the binary vesicles is determined by the degree of dissimilarity that is effectively captured by the soft repulsive interaction parameters a_{h1h2} , a_{t1t2} , as shown in Fig. 2 (a) – (c) and Fig. 3 (a) – (c). We have selected the range for the parameters a_{h1h2} , and a_{t1t2} to induce phase segregation of the lipid species while avoiding budding and vesiculation processes on the vesicle bilayer.¹⁵ All the results have been averaged using particle trajectories from four simulations that begin from the same initial conditions but have different random seeds.

We characterize the coarsening dynamics in a two-component lipid bilayer by measuring the number of clusters or domains composed of a given lipid specie, as a function of time (beginning from the mixed state, as shown in Fig. 1 (b).) We define a cluster to be composed of lipids from a given species whose head group beads are within interaction range from each other. This definition of a cluster enables us to distinguish between the clusters formed in the two monolayers. The lipid molecules in the inner monolayer are more closely packed as the inner monolayer occupies a spherical shell of smaller volume than the outer monolayer.⁷² The difference in the occupied volumes is reflected in the asymmetry in the number of clusters in the two monolayers, as we observe fewer clusters in the inner monolayer. Our measurements of the time evolution of the cluster count show the cluster growth to be influenced by the degree of dissimilarity between the lipid species, as shown in Figs. 2 (d) and 3 (d). We observe the interfacial tension to increase with the dissimilarity between the lipid species, thereby inducing the phase segregation process to minimize the interfacial tension by forming fewer clusters of a given lipid species. Given the higher number of tail beads per lipid molecule, the interfacial tension for systems containing lipid molecules with distinct hydrocarbon tail groups is greater than those with different head groups. Hence, for identical values of the soft repulsion parameters a_{h1h2} and a_{t1t2} , we report fewer clusters for lipid mixtures with distinct tail groups.^{31,73}

For sufficiently low interfacial tensions, the thermal fluctuations of the bilayer can dominate the energetically favorable interactions between the like lipid species to cause fragmentation of the clusters. Variations in the cluster count are observed to occur due to the high mobility of the lipid molecules between two successive time steps. Supplementary Information SI.1 demonstrates the rapid changes in the positions of the lipid head beads for four consecutive time steps. Therefore, the coalescence or fragmentation of clusters can be induced by factors such as thermal fluctuations of the bilayer and lipid mobility. For temperature dependent phase segregation in multicomponent bilayers, studies^{13,26,27} have shown the coarsening dynamics to be determined by the characteristic correlation length of the fluctuations of the domain boundaries and the hydrodynamic radius, for temperatures below the critical demixing value.

The coarsening dynamics process can also be characterized through the time evolution of the average size of the clusters, as shown in Figs. 2 (e) and 3 (e). We define the size of a cluster to be given by the total number of molecules of a given lipid species that comprises a cluster. We expect higher values of the line tension between the dissimilar components to result in the rapid formation of fewer but larger-sized clusters. We find the measurements to support our expectations and report the trends in the time evolution of the average cluster size to be inverse to those for the number of clusters.^{16,74,75} We have summarized our observed trends of the aggregate size as a function of the distinction between the head and the tail groups in Fig. 4.

We would like to note that the error bars are calculated based on the standard deviation of the results over four different random seeds. We find large error bars for the higher values of the soft repulsive interaction parameters between the tail beads of the two lipid species (see Fig. 3 (e).) A plausible explanation for the large error bars is the presence of very few clusters (corresponding to the very large average cluster sizes) at the high soft repulsive interaction parameters of the tail beads. For example, when we use very high soft repulsive interaction parameter such as $a_{t1t2} = 50$, we observe a highly segregated vesicle which has, on the average, two to four clusters of a specific lipid type. Our measurements for the number of clusters,

average cluster size and the corresponding standard deviations are computed using smaller number of samples.

The time evolution of the coarsening dynamics can be used to compute the scaling exponent of the clustering process by using the following relation $N(t) \sim C t^\alpha$, where $N(t)$ is the number of clusters, C is a constant, t is time, and α is the scaling exponent. Similarly, the growth in the average size of a cluster can be characterized by using the following relation $\langle S(t) \rangle \sim D t^\beta$, where $\langle S(t) \rangle$ is the average size of the clusters, D is a constant, t is time, and β is the scaling exponent. Table 2 provides the scaling exponents α and β for the values of the soft repulsive interaction parameters a_{112} which result in macroscopic phase segregation. The cluster number and the average cluster size scaling exponents demonstrate inverse trends with increasing dissimilarity of the lipid species. The average cluster size measurements can be used to calculate the time evolution of the average area of the clusters $\langle A(t) \rangle$ through the average area per lipid a_{lipid} , corresponding to a given soft repulsion interaction parameter (as shown Table 3.) The average area of the clusters $A(t)$ can be demonstrated to have a similar scaling behavior as the average cluster size using the following approximations $\langle A(t) \rangle \sim a_{lipid} \langle S(t) \rangle \sim a_{lipid} D t^\beta \propto t^\beta$. If we assume the clusters to be a circle with an average radius $R(t)$, then $\langle A(t) \rangle \propto R(t)^2$ and $R(t) \propto t^{\beta/2}$. If the total interface length $L(t)$ of the clusters is given by $N(t) 2 \pi R(t)$ and the A_{total} is the total area occupied by the clusters of a given species, $R(t) \sim A_{total}/L(t)$.^{4,14} Our measurements of the scaling exponents, as detailed in Table 2, are in agreement with earlier numerical and experimental results^{4,14-17,22} showing $N(t) \propto t^{-2/3}$, $L(t) \propto t^{-1/3}$ and $R(t) \propto t^{1/3}$. A growth exponent for the average radius of 1/3 is usually attributed to the evaporation-condensation effect.^{4,14,16,76} Our simulations have also demonstrated the domain dynamics at the latter stages to be determined by the diffusion and collisions of the clusters. We have provided the plots of the time evolution of the number of clusters and the average cluster size used to compute the scaling exponents in the Supplementary Information SI.2 and SI.3.

The packing of the lipid molecules in the vesicle bilayer is not very sensitive to differences in the head or tail groups, and can be characterized by the bilayer thickness and the area per lipid, as shown in Table 3. To calculate the bilayer thickness, the vesicle is divided into 128 patches so that each patch can be treated effectively as a bilayer membrane. The bilayer thickness is computed by measuring the distance between the lipid head groups in the opposing monolayers, in a given patch. These measurements were computed using the particle configurational data obtained from four simulations using identical initial conditions but different random seeds. The bilayer distance was measured for each patch and was averaged over all the patches, the particle configurational snapshots and the different random seeds. The area per lipid was measured using the approach detailed in the *Methodology* section.

The phase segregation on the vesicle bilayer is driven by the thermodynamics of the system. We draw correspondence between the degree of phase segregation and thermodynamic properties by measuring the interfacial line tension and surface tension of the lipid vesicles, for the different tail-tail interaction parameters. The measurements are performed on equilibrium configurations of the binary mixtures, for a range of dissimilarities between the tail groups of the two lipid species. The line tension of an interface separating two phases can be found by calculating the excess free energy per unit length of the contact length along the interface.⁷⁷ We estimate the line tension λ of the domain boundary through the following equation⁷⁸ $\lambda \equiv$

$\left[\frac{1}{2} (U_{AA} + U_{BB}) - U_{AB} \right] / l_{mo}$, where U_{AA} , U_{BB} , and U_{AB} are the pair interaction energies between components A and B, and l_{mo} is the lateral size of the lipid molecules. The lateral size of the lipid molecules is given by $1.1r_c$ from the area per lipid calculation provided in the *Methodology* section. The results for the line tension measurements as a function of the soft repulsive interaction parameter a_{11-12} are found to be consistent with our observations of the coarsening dynamics (see Fig. 5), and have been averaged over all particles in the system. Our results for the line tension are in agreement with theoretical^{26,79} and experimental²⁶ studies which demonstrate the interfacial line tension to increase with an order parameter which characterizes the degree of phase segregation. According to the theory proposed by Schick et al.,⁷⁹ there are two key factors which control the phase segregation in multi-component lipid membranes. One of the factors is the repulsive interaction between dissimilar lipid molecules (such as a mixture of saturated and unsaturated lipid molecules) which depends on the magnitude of the order parameter. The order parameter is used in the theory to provide a measure of the degree of order for the saturated lipid chains. As the order parameter increases, the repulsive interactions between the saturated and unsaturated lipid molecules will increase, which results in phase segregation. This effect is analogous to increasing the soft repulsive interaction parameter a_{ij} between the hydrocarbon tail groups of the dissimilar lipid species in our simulations. The other factor is the addition of cholesterol-like sterols which results in ordering in the saturated lipid chains, thereby inducing phase segregation. The second factor is not relevant for our investigation as we do not include sterols in our system.

The second thermodynamic property we investigate is the surface tension of the binary lipid vesicle by computing the difference between the internal and external pressures of the bilayer.⁸⁰⁻⁸² The relation between the surface tension and pressure difference across the vesicle bilayer has been shown to be given by Laplace's law which requires the following equation to hold: $P_N(r_i) - P_N(r_j) = \frac{2\gamma_{ij}}{r_i}$ ⁸² where r_i and r_j are the distances of the centers of mass of the particles in the inner and outer monolayers of the vesicle from the center of the vesicle, $P_N(r_i)$ and $P_N(r_j)$ are the normal components of the pressure in the two monolayers, and γ_{ij} is macroscopic surface tension. We compute the normal pressure components by measuring the stress tensor for each bead in the bilayer of the vesicle^{83,84} The stress tensor is given by $\Sigma^{\alpha\beta} = \begin{pmatrix} \Sigma_T & 0 & 0 \\ 0 & \Sigma_T & 0 \\ 0 & 0 & \Sigma_N \end{pmatrix}$ from where the diagonal component $\Sigma^{\alpha\beta}$ is extracted for each bead and is correlated with its distance from center of the vesicle. The normal component of the pressure can be calculated by summing over the normal component of the stress tensor for each bead, and normalizing by the system volume. In order to calculate $P_N(r_i)$ and $P_N(r_j)$, we measure the normal pressure on the lipid head beads in the inner and outer monolayers. By using Laplace's law, we compute the surface tension as a function of the soft repulsive interaction parameter a_{11-12} as shown in Fig. 6. For all the values of the soft repulsive interaction parameters examined, we find the average inner pressure to be greater than the average outer pressure which results in a positive surface tension. We observe the surface tension to decrease as the soft repulsive interaction parameter between the tail groups of the different lipid species increases. This finding is consistent with the trends in the area per lipid as a function of the soft repulsive interaction parameter, as shown in Table 3. We observe the surface tension to decrease at higher values of a_{11-12} ($41 k_b T/r_c$ and $50 k_b T/r_c$) with corresponding increases in the area per lipid, as shown in Fig.

6. A possible explanation for this observation could be an increase in the interstitial space between the two phases as a consequence of the strong repulsive interactions between the tail groups of the two lipid species. The repulsive interaction would increase the fluid flux from the inside to the outside of the vesicle, thereby decreasing the pressure difference, and the surface tension. We would also like to note that theoretical⁸⁵ and experimental⁸⁶ studies have also demonstrated tension to increase the degree of phase segregation in lipid membranes.

We have also explored the role of hydrophobic tail stiffness on the phase segregation of a two-component lipid vesicle. The stiffness of the hydrocarbon tails of lipid molecules is dependent upon their length and saturation.⁸⁷⁻⁸⁹ Lipid molecules with shorter hydrocarbon tails have lower stiffness and viscosity as they are more susceptible to changes in kinetic energy.⁸⁷⁻⁸⁹ Unsaturated lipid molecules are unable to pack as tightly as saturated lipid molecules due to the kinks in their hydrocarbon tails, and are therefore more susceptible to changes in kinetic energy. An experimental example of a saturated lipid molecular species with stiffer tails is 1,2-distearoyl-*sn*-glycero-3-phosphocholine (18 carbon atoms⁹⁰) We would like to note that the DPPC molecule is a saturated phospholipid with 16 carbon atoms in each hydrocarbon tail.

We began with a completely mixed binary vesicle (as shown in Fig. 1 (b)) and ran the simulations for an interval 5000τ using a desired value of the hydrophobic tail angle coefficient $K_{angle,1}$ of one of the lipid species. The interfacial tension arising from the differences in the tail stiffness of the molecular species was sufficiently small so as to prevent macroscopic phase segregation (see Fig. 7 (a) – (d).) However, the shape of the vesicle is observed to evolve from an ellipsoidal to a spherical morphology with increasing chain stiffness of one of the lipid species. The vesicle stabilizes to a spherical shape for values of chain stiffness parameter $K_{angle,1}$ set at 10ϵ or higher, as shown in Fig. 7 (d).

The effect of chain stiffness on molecular packing of the lipids in the bilayer can be characterized through the measurement of the area per lipid. Using a similar approach to that detailed in the *Methodology* section, we measure the average area per lipid for different values of the chain stiffness. We observe the lipid molecules to become more tightly packed as the chain stiffness of one of the species increases due to fewer molecular conformations sampled and smaller excluded volumes, for values of $K_{angle,1}$ set at 10ϵ or higher, as shown in Fig. 7 (e).

We also investigate the effect of shape change on the surface tension by measuring the surface tension of the vesicle with ellipsoidal morphology as shown on Fig. 7 (a). We find that the surface tension of the ellipsoidal-shaped vesicles reduces to approximately half of the surface tension for spherical-shaped vesicles. This result is consistent with the observation that increases in the surface tension makes the vesicles more spherical in shape.⁸⁰ In addition, experimental investigations have shown mitotic cells to transform into a spherical shape by increasing their surface tension to accelerate the epithelial invagination process.⁹¹

CONCLUSIONS

In summary, we have demonstrated the coarsening dynamics in a binary vesicle composed of two-tail lipid molecules with different chemical properties. In the early stages of the phase segregation process, the lipid molecules of the same species formed small clusters or domains via diffusion and collision to minimize their interfacial tension. For the latter stages, as

the domains grow in size the clustering dynamics is determined by the diffusion and collision of clusters, and the evaporation of individual lipids from the boundaries of small clusters and their coalescence into bigger clusters. We observe the first stage for lipid mixtures with low interfacial energies or smaller degree of dissimilarity between the lipid species. For higher interfacial tension between the distinct lipid species, we demonstrate both stages through the characterization of the clustering dynamics. Our measurements of the growth exponents for systems demonstrating macroscopic phase segregation agree with earlier numerical and experimental studies.^{4,14-17,22} We did not observe significant changes in the bilayer thickness and the area per lipid for different mixtures of lipid species. Our measurements of the line tension are consistent with theoretical and experimental studies.^{26,79} In addition, we observe the surface tension calculations to support our trends in the average area per lipid as function of the dissimilarity between the lipid species. Finally, the molecular chain stiffness of the hydrophobic tail groups was found to determine the shape of the binary vesicle, but had no noticeable effect on the phase segregation process. These results can be used to develop simple models of bio-inspired membranes with tunable phase segregation properties to design material platforms for applications in drug delivery, sensing and sustainability.

ACKNOWLEDGEMENTS

The authors would like to acknowledge the use of high performance computational resources at the Rutgers Engineering Computational Cluster (<http://linuxcluster.rutgers.edu/>) and Rutgers Discovery Informatics Institute (<http://rdi2.rutgers.edu/>).

REFERENCES

- 1 L. H. Gao, J. Shillcock and R. Lipowsky, Improved dissipative particle dynamics simulations of lipid bilayers, *J. Chem. Phys.*, 2007, **126**, 015101.
- 2 B. Alberts, A. Johnson, J. Lewis, M. Raff, K. Roberts and P. Walter, Molecular biology of the cell, *Garland Science*, New York, 2007.
- 3 J. C. Shillcock and R. Lipowsky, Equilibrium structure and lateral stress distribution of amphiphilic bilayers from dissipative particle dynamics simulations, *J. Chem. Phys.*, 2002, **117**, 5048–5061.
- 4 M. Laradji and P.B.S. Kumar, Dynamics of domain growth in self-assembled fluid vesicles, *Phys. Rev. Lett.*, 2004, **93**, 198105.
- 5 R. Lipowsky and E. Sackmann, Structure and dynamics of membranes, Handbook of biological physics, *Elsevier*, Amsterdam, 1995.
- 6 J. Israelachvili, Intermolecular and surface forces, *Academic Press*, Boston, 2011.
- 7 E. Koufos, B. Muralidharan and M. Dutt, in preparation.
- 8 J.L.R. Rubenstein, B.A. Smith, and H.M. McConnell, Lateral diffusion in binary mixtures of cholesterol and phosphatidylcholines, *Proc. Natl. Acad. Sci. USA*, 1979, **76**, 15-18.
- 9 N. Kahya, D. Scherfeld and P. Schwille, Differential lipid packing abilities and dynamics in giant unilamellar vesicles composed of short-chain saturated glycerol-phospholipids, sphingomyelin and cholesterol, *Chem. Phys. Lipids*, 2005, **135**, 169–180.
- 10 Z. V. Leonenko, E. Finot, H. Ma, T. E. S. Dahms and D. T. Cramb, Investigation of temperature-induced phase transitions in DOPC and DPPC phospholipid bilayers using temperature-controlled scanning force microscopy, *Biophys. J.*, 2004, **86**, 3783–3793.

- 11 S. L. Veatch and S. L. Keller, Separation of liquid phases in giant vesicles of ternary mixtures of phospholipids and cholesterol, *Biophys. J.*, 2003, **85**, 3074–3083.
- 12 R. Lipowsky, Budding of membranes induced by intramembrane domains, *J. Phys. II*, 1992, **2**, 1825.
- 13 C. Esposito, A. Tian, S. Melamed, C. Johnson, S-Y. Tee and T. Baumgart, Flicker spectroscopy of thermal lipid bilayer domain boundary fluctuations, *Biophys. J.*, 2007, **93**, 3169-3181.
- 14 M. Laradji and P.B.S. Kumar, Domain growth, budding, and fission in phase separating self-assembled fluid bilayers, *J. Chem. Phys.*, 2005, **123**, 224902.
- 15 S. Ramachandran, M. Laradji and P.B.S. Kumar, Lateral organization of lipids in multi-component liposomes, *J. Phys. Soc. Jpn.*, 2009, **78**, 041006.
- 16 C.A. Stanich, A.R. Honerkamp-Smith, G.G. Putzel, C.S. Warth, A.K. Lamprecht, P. Mandal, E. Mann, T.-A.D. Hua and S.L. Keller, Coarsening dynamics of domains in lipid membranes, *Biophys. J.*, 2013, **105**, 444-454.
- 17 T. Taniguchi, Shape deformation and phase separation dynamics of two-component vesicles, *Phys. Rev. Lett.*, 1996, **76**, 4444-4447.
- 18 J. Fan, T. Han and M. Haataja, Hydrodynamic effects on spinodal decomposition kinetics in planar lipid bilayer membranes, *J. Chem. Phys.*, 2010, **133**, 235101.
- 19 L.A. Bagatolli and E. Gratton, Direct observation of lipid domains in free standing bilayers using two-photon excitation fluorescence microscopy, *J. of Fluorescence*, 2001, **11**, 141-160.
- 20 S. Ramachandran, S. Komura and G. Gompper, Effects of an embedding bulk fluid on phase separation dynamics in a thin liquid film, *EPL*, 2010, **89**, 56001.
- 21 T.S. Ursell, W.S. Klug and R. Phillips, Morphology and interaction between lipid domains, *Proc. Lateral Organization of Lipids in Multi-component Liposomes Natl. Acad. Sci. USA*, 2009, **106**, 13301.
- 22 L. Bagatolli and P.B.S. Kumar, Phase Behavior of multicomponent membranes: Experimental and computational techniques, *Soft Matter*, 2009, **5**, 3234-3248.
- 23 I. R. Cooke, K. Kremer and M. Deserno, Tunable generic model for fluid bilayer membranes, *Phys. Rev. E*, 2005, **72**, 011506.
- 24 S. J. Marrink, A. H. de Vries and D. P. Tieleman, Lipids on the move: Simulations of membrane pores, domains, stalks and curves, *Biochim. Biophys. Acta, Biomembr.*, 2009, **1788**, 149–168.
- 25 Simons, K., and D. Toomre, Lipid rafts and signal transduction, *Nat. Rev. Mol. Cell. Biol.*, 2000, **1**, 31-39.
- 26 A.R. Honerkamp-Smith, P. Cicuta, M.D. Collins, S.L. Veatch, M. den Nijs, M. Schick and S.L. Keller, Line tensions, correlation lengths, and critical exponents in lipid membranes near critical points, *Biophys. J.*, 2008, **95**, 236-246.
- 27 A. R. Honerkamp-Smith, S. L. Veatch and S. L. Keller, An introduction to critical points for biophysicists; observations of compositional heterogeneity in lipid membranes, *Biochim. Biophys. Acta*, 2009, **1788**, 53-63.
- 28 F. L. H. Brown, Continuum simulations of biomembrane dynamics and the importance of hydrodynamic effects, *Q. Rev. Biophys.*, 2011, **44**, 391–432.
- 29 M. Laradji and P. B. Kumar, Anomalously slow domain growth in fluid membranes with asymmetric transbilayer lipid distribution, *Phys. Rev. E: Stat., Nonlinear, Soft Matter Phys.*, 2006, **73**, 040910(R).
- 30 G. Illya, R. Lipowsky and J. C. Shillcock, Two-component membrane material properties and domain formation from dissipative particle dynamics, *J. Chem. Phys.*, 2006, **125**, 114710.
- 31 P.B.S. Kumar, G. Gompper and R. Lipowsky, Budding dynamics of multicomponent membranes, *Phys. Rev. Lett.*, 2000, **86**, 3911-3914.
- 32 P.B.S. Kumar and M. Rao, Kinetics of phase ordering in a two component fluid membrane, *Mol. Cryst. Liq. Cryst.*, 1996, **288**, 105.
- 33 R. D. Groot, P. B. Warren, Dissipative Particle Dynamics: Bridging the gap between atomistic and mesoscopic simulation, *J. Chem. Phys.*, 1997, **107**, 4423–4435.

- 34 K. A. Smith, D. Jasnow and A. C. Balazs, Designing synthetic vesicles that engulf nanoscopic particles, *J. Chem. Phys.*, 2007, **127**, 084703.
- 35 A. Alexeev, W. E. Upsal and A. C. Balazs, Harnessing janus nanoparticles to create controllable pores in membranes, *ACS Nano*, 2008, **2**, 1117–1122.
- 36 X. Yong, E. J. Crabb, N. M. Moellers, and A. C. Balazs, Self-healing vesicles deposit lipid-coated janus particles into nanoscopic trenches, *Langmuir*, 2013, **29**, 16066–16074.
- 37 I. Salib, X. Yong, E. J. Crabb, N. M. Moellers, G. T. MacFarlin, O. Kuksenok, A. C. Balazs, Harnessing fluid-driven vesicles to pick up and drop off Janus particles, *ACS Nano*, 2013, **7**, 1224–1238.
- 38 Z. G. Mills, W. Mao, A. Alexeev, Mesoscale modeling: solving complex flows in biology and biotechnology, *Trends Biotechnol.*, 2013, **31**, 426–434.
- 39 H. Masoud and A. Alexeev, Controlled release of nanoparticles and macromolecules from responsive microgel capsules, *ACS Nano*, 2012, **6**, 212–219.
- 40 H. Masoud and A. Alexeev, Selective control of surface properties using hydrodynamic interactions, *Chem. Commun.*, 2010, **47**, 472–474.
- 41 M. Dutt, M.J. Nayhouse, O. Kuksenok, S.R. Little and A.C. Balazs, Interactions of end-functionalized nanotubes with lipid vesicles: Spontaneous insertion and nanotube self-organization, *Current Nanoscience*, 2011, **7**, 699–715.
- 42 M. Dutt, O. Kuksenok, M.J. Nayhouse, S.R. Little and A.C. Balazs, Modeling the self-assembly of lipids and nanotubes in solution: Forming vesicles and bicelles with transmembrane nanotube channels, *ACS Nano*, 2011, **5**, 4769–4782.
- 43 M. Dutt, O. Kuksenok, S.R. Little and A.C. Balazs, Forming transmembrane channels using end-functionalized nanotubes, *Nanoscale*, 2011, **3**, 240–250.
- 44 M. Dutt, O. Kuksenok, S.R. Little and A.C. Balazs, Designing tunable bio-nanostructured materials via self-assembly of amphiphilic lipids and functionalized nanotubes, *MRS Spring 2012 Conference Proceedings*, 2012, 1464.
- 45 M. Dutt, O. Kuksenok, and A.C. Balazs, Nano-pipette directed transport of nanotube transmembrane channels and hybrid vesicles, *Nanoscale*, 2013, **5**, 9773–9784.
- 46 Chou, H.-K. Tsao and Y.-J. Sheng, Morphologies of multicompartment micelles formed by triblock copolymers, *J. Chem. Phys.*, 2006, **125**, 194903.
- 47 V. Ortiz, S. O. Nielsen, D. E. Discher, M.L. Klein, R. Lipowsky and J. Shillcock, Dissipative Particle Dynamics simulations of polymerosome, *J. Phys. Chem. B*, 2005, **109**, 17708 – 17714.
- 48 E.S. Boek, P.V. Coveney, H.N.W. Lekkerkerker and P. van der Schoot, Simulating rheology of dense colloidal suspensions using dissipative particle dynamics, *Phys. Rev. E*, 1997, **55**, 3124 – 31.
- 49 N.A. Spenley, Scaling laws for polymers in dissipative particle dynamics, *Europhys. Lett.*, 2000, **49**, 534–540.
- 50 X. Fan, N. Phan-Thien, S. Chen, X. Wu and T.Y. Ng, Simulating flow of DNA suspension using dissipative particle dynamics, *Phys. Fluids*, **18**, 2006, 063102.
- 51 S. Chem, N. Phan-Thien, X.J. Fan and B.C. Khoo, Dissipative particle dynamics of polymer drops in periodic shear flow, *J. Non-Newtonian Fluid Mech.*, 2004, **118**, 65 – 81.; 43.
- 52 S. Yamamoto, Y. Maruyama and S. Hyodo, Dissipative particle dynamics study of spontaneous vesicle formation of amphiphilic molecules, *J. Chem. Phys.*, 2002, **116**, 5842 – 5849.
- 53 M. Kranenburg, M. Venturoli, and B. Smit, Phase behavior and induced interdigitation in bilayers studied with dissipative particle dynamics, *J. Phys. Chem.*, 2003, **41**, 11491.
- 54 M. Kranenburg, C. Laforge and B. Smit, Mesoscopic simulations of phase transitions in lipid bilayers, *Phys. Chem. Chem. Phys.*, 2004, **6**, 4531–4534.
- 55 M. Kranenburg and B. Smit, Phase behavior of model lipid bilayers, *J. Phys. Chem. B*, 2005, **109**, 6553 – 6563.
- 56 M. Kranenburg, M. Vlaar and B. Smit, Simulating induced interdigitation in membranes, *Biophys J.*, 2004, **87**, 1596–1605.

- 57 P. K. Depa and J. K. Maranas, Dynamic evolution in coarse-grained molecular dynamics simulations of polyethylene melts, *J. Chem. Phys.*, 2007, **126**, 054903.
- 58 S. V. Bennuna, M. I. Hoopesb, C. Xingc and R. Faller, Coarse-grained modeling of lipids, *Chemistry and Physics of Lipids*, 2009, **159**, 59–66.
- 59 S. J. Marrink, J. Risselada and A. E. Mark, Simulation of gel phase formation and melting in lipid bilayers using a coarse grained model, *Chemistry and Physics of Lipids*, 2005, **135**, 223–244.
- 60 M. J. Stevens, Coarse-grained simulations of lipid bilayers, *J. Chem. Phys.*, 2004, **121**, 11942.
- 61 T. Harder, Formation of functional cell membrane domains: the interplay of lipid- and protein-mediated interactions, *Philos. Trans. R. Soc. London*, 2003, **358**, 863–868.
- 62 K. Simons, J. L. Sampaio, Membrane organization and lipid rafts, *Cold Spring Harb. Perspect. Biol.*, 2011, **3**, 1–17.
- 63 D. A. Brown and E. London, Structure and origin of ordered lipid domains in biological membranes, 1998, *J. Membr. Biol.*, **164**, 103–114.
- 64 K. Khairy and J. Howard, Minimum-energy vesicle and cell shapes calculated using spherical harmonics parameterization, *Soft Matter*, 2011, **7**, 2138.
- 65 H. Lei and G.E. Karniadakis, Predicting the morphology of sickle red blood cells using coarse-grained models of intracellular aligned hemoglobin polymers, *Soft Matter*, 2012, **8**, 4507–4516.
- 66 M.P. Allen and D.J. Tildesley, Computer simulations of liquids, *Clarendon Press*, Oxford, 2001.
- 67 A. Imparato, J. C. Shillcock and R. Lipowsky, Lateral and transverse diffusion in two-component bilayer membranes, *Eur. Phys. J. E*, 2003, **11**, 21–28.
- 68 J. Hu, T. Weigl and R. Lipowsky, Vesicles with multiple membrane domains, *Soft Matter*, 2011, **7**, 6092.
- 69 J. F. Nagle and S. Tristram-Nagle, Structure of Lipid Bilayers, *Biochim. Biophys. Acta*, 2000, **1469**, 159.
- 70 D. Frenkel and B. Smit, Understanding molecular simulations: From algorithms to applications, *Academic Press*, San Diego, 2002.
- 71 P. Ludford, F. Aydin and M. Dutt, Design and characterization of nanostructured biomaterials via the self-assembly of lipids, *MRS Fall 2013 Conference Proceedings*, 2013, 1498.
- 72 M.K. Campbell and O.F. Shawn, Biochemistry, *Brooks/Cole Cengage Learning*, Belmont, CA, 2012.
- 73 X. Liang, L. Li, F. Qiu and Y. Yang, Domain growth dynamics in multicomponent vesicles composed of BSM/DOPC/cholesterol, *Physica A*, 2010, **389**, 3965–3971.
- 74 D. Saeki, T. Hamada and K. Yoshikawa, Domain-Growth Kinetics in a Cell-Sized Liposome, *J. Phys. Soc. Jpn.*, 2006, **75**, 013602.
- 75 M. Yanagisawa, M. Imai, T. Masui, S. Komura and T. Ohta, Growth dynamics of domains in ternary fluid vesicles, *Biophys. J.*, 2007, **92**, 115–125.
- 76 I. M. Lifshitz and V. V. Slyozov, The kinetics of precipitation from supersaturated solid solutions, *J. Phys. Chem. Solids*, 1961, **19**, 35–50.
- 77 J. H. Weijs, A. Marchand, B. Andreotti, D. Lohse, and J. H. Snoeijer, Origin of line tension for a Lennard-Jones nanodroplet, *Phys. Fluids*, 2011, **23**, 022001.
- 78 Reinhard Lipowsky and Rumiana Dimova, Domains in membranes and vesicles, *J. Phys.: Condens. Matter*, 2003, **15**, 31–45.
- 79 G. G. Putzel and M. Schick, Phenomenological model and phase behavior of saturated and unsaturated lipids and cholesterol, *Biophys. J.*, 2008, **95**, 4756–4762.
- 80 R. Glaser, Biophysics, *Springer*, Berlin, 1996.
- 81 C. Tanford, Hydrostatic pressure in small phospholipid vesicles, *Proc. Nati. Acad. Sci. USA*, 1979, **76**, 3318–3319.
- 82 S. H. White, Small phospholipid vesicles: Internal pressure, surface tension, and surface free energy, *Proc. Nati. Acad. Sci. USA*, 1980, **77**, 4048–4050.

- 83 R. Goetz and R. Lipowsky, Computer simulations of bilayer membranes: Self-assembly and interfacial tension, *J. Chem. Phys.*, 1998, **108**, 7397.
- 84 P. Schofield and J. R. Henderson, Statistical mechanics of inhomogeneous fluids, *Proc. R. Soc. London Ser. A*, 1982, **379**, 231.
- 85 M. J. Uline, M. Schick and I. Szleifer, Phase behavior of lipid bilayers under tension, *Biophys. J.*, 2012, **102**, 517–522.
- 86 T. Hamada, Y. Kishimoto, T. Nagasaki and M. Takagi, Lateral phase separation in tense membranes, *Soft Matter*, 2011, **7**, 9061.
- 87 G. Illya, R. Lipowsky and J. C. Shillcock, Effect of chain length and asymmetry on material properties of bilayer membranes, *J. Chem. Phys.*, 2005, **122**, 244901.
- 88 W. Rawicz, K. C. Olbrich, T. McIntosh, D. Needham and E. Evans, Effect of chain length and unsaturation on elasticity of lipid bilayers, *Biophys. J.*, 2000, **79**, 328–339.
- 89 I. Szleifer, D. Kramer, A. Ben-Shaul, D. Roux and W. M. Gelbart, Curvature elasticity of pure and mixed surfactant films, *Phys. Rev. Lett.*, 1988, **60**, 1966-1969.
- 90 N. Kučerka, M. P. Nieh and J. Katsaras, Fluid phase lipid areas and bilayer thicknesses of commonly used phosphatidylcholines as a function of temperature, *J. Biochim. Biophys. Acta*, 2011, **1808**, 2761–2771.
- 91 T. Kondo and S. Hayashi, Mitotic cell rounding accelerates epithelial invagination, *Nature*, 2013, **494**, 125–129.
- 92 E. Koufos, B. Muralidharan and M. Dutt, Computational Design of Multi-component Bio-Inspired Bilayer Membranes, *AIMS Materials Science*, 2014, **103**, 103-120.
- 93 Lipid bilayer thickness varies linearly with acyl chain length in fluid phosphatidylcholine vesicles, *J. Mol. Biol.*, 1983, **166**, 211-217.
- 94 S. E. Feller, R. M. Venable and R. W. Pastor, Computer simulation of a DPPC phospholipid bilayer: Structural changes as a function of molecular surface area, *Langmuir*, 1997, **13**, 6555-6561.
- 95 G. Brannigan, P.F. Philips and F.L.H. Brown, Flexible lipid bilayers in implicit solvent, *Phys. Rev. E*, 2005, **72**, 011915.
- 96 D. E. Discher, V. Ortiz, G. Srinivas, M. L. Klein, Y. Kim, D. Christian, S. Cai, P. Photos and F. Ahmed, Emerging applications of polymersomes in delivery: From molecular dynamics to shrinkage of tumors, *Prog. Polym. Sci.*, 2007, **32**, 838 – 857.

Figure Captions

Figure 1: (a) The amphiphilic lipid molecules, (b) completely mixed binary component lipid vesicle at $t = 10,000\tau$.

Figure 2: Snapshots from the final configurations of the binary component lipid vesicle at $t = 5,000\tau$ for different soft repulsive interaction parameters between the head groups of the two lipid species (a) $a_{h_1-h_2} = 26$, (b) $a_{h_1-h_2} = 42$, (c) $a_{h_1-h_2} = 50$. All the simulations start from the completely mixed state. (d) A plot of the time evolution of the total number of clusters of one type of lipid after a single stable vesicle has formed for the head-head soft repulsive interaction parameters of $a_{h_1-h_2} = 26, 34, 42, \text{ and } 50$. (e) A plot of the time evolution for the average cluster size of one type of lipid after a single stable vesicle has formed for the head-head soft repulsive interaction parameters of $a_{h_1-h_2} = 26, 34, 42, \text{ and } 50$. The simulations have been run for a total time of $10,000\tau$ from the mixed state and each data point has been averaged over four simulation runs using different random seeds.

Figure 3: Snapshots from the final configurations of the binary component lipid vesicle at $t = 5,000\tau$ for different soft repulsive interaction parameters between the tail groups of the two lipid

species (a) $a_{t1-t2} = 26$, (b) $a_{t1-t2} = 29$, (c) $a_{t1-t2} = 31$. All the simulations start from the completely mixed state. (d) A plot of the time evolution of the total number of clusters of one type of lipid after a single stable vesicle has formed for the tail-tail soft repulsive interaction parameters of $a_{t1-t2} = 26, 27, 28, 29, 30, 31, 32, 41, \text{ and } 50$. (e) A plot of the time evolution for the average cluster size of one type of lipid after a single stable vesicle has formed for the tail-tail soft repulsive interaction parameters of $a_{t1-t2} = 26, 27, 28, 29, 30, 31, 32, 41, \text{ and } 50$. The simulations have been run for a total time of $10,000\tau$ from the mixed state and each data point has been averaged over four simulation runs using different random seeds.

Figure 4: A plot of the aggregate size as a function of the soft repulsion interaction parameters between (a) the head groups (a_{h1h2}) and (b) the tail groups (a_{t1t2}). The simulations have been run for a total time of $10,000\tau$ from the mixed state and each data point has been averaged over four simulation runs using different random seeds.

Figure 5: A plot of the average line tension as a function of the tail-tail soft repulsive interaction parameters a_{t1-t2} ($= 26, 27, 28, 29, 30, 31, 32, 41, \text{ and } 50$.) The measurements were performed on particle trajectories starting at $10,000\tau$, for a total duration of $5,000\tau$. Each data point has been averaged over time.

Figure 6: A plot of the surface tension as a function of the tail-tail soft repulsive interaction parameters a_{t1-t2} ($= 26, 27, 28, 29, 30, 31, 32, 41, \text{ and } 50$.) The measurements were performed on particle trajectories starting at $10,000\tau$, for a total interval of $25,000\tau$. We adopt a box averaging approach to compute the errors.⁹²

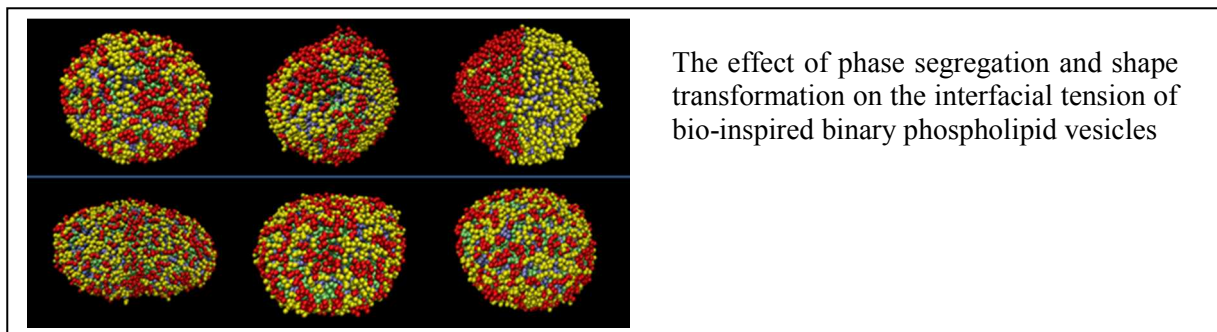
Figure 7: Snapshots from the final configurations of the binary component lipid vesicle at $t = 5,000\tau$ while keeping the angle coefficient of one type of lipid at a constant value of $K_{angle,2} = 20$ and varying the angle coefficient of other type of lipid for the values of (a) $K_{angle,1} = 0$, (b) $K_{angle,1} = 5$, (c) $K_{angle,1} = 10$, (d) $K_{angle,1} = 15$. All the simulations start from the completely mixed state. (e) The area per lipid of the binary component vesicle as the angle coefficient of specific type of lipid species ($K_{angle,1}$) is varied from 0 to 40 and the angle coefficient of other type of lipid species is kept at a constant value of $K_{angle,2} = 20$. The simulations have been run for a total time of $5,000 \tau$.

Table Captions

Table 1: The soft repulsive interaction parameters, a_{ij} between head, tail beads of lipid type 1 and 2 and the solvent beads. The boxes with “—” represent the interaction parameters that can be varied for the mixture of lipids with different chemical properties.

Table 2: Table of the scaling exponents α (obtained from the measurements of number of clusters) and β (obtained from the measurements of the average cluster size) for different soft repulsive interaction parameters of the tail groups of the two lipid species, $a_{t1-t2} = 31, 32, 41, \text{ and } 50$. The simulations used to obtain the scaling exponents have been run for a total time of $10,000\tau$ and averaged over four different random seeds.

Table 3: The bilayer thickness and area per lipid of the binary component vesicle as a function of different soft repulsive interaction parameters between the tail groups of the two lipid species, $a_{t1-t2} = 31, 32, 41, \text{ and } 50$. The simulations have been run for a total time of $10,000 \tau$ and each data point has been averaged over four simulation runs using different random seeds.



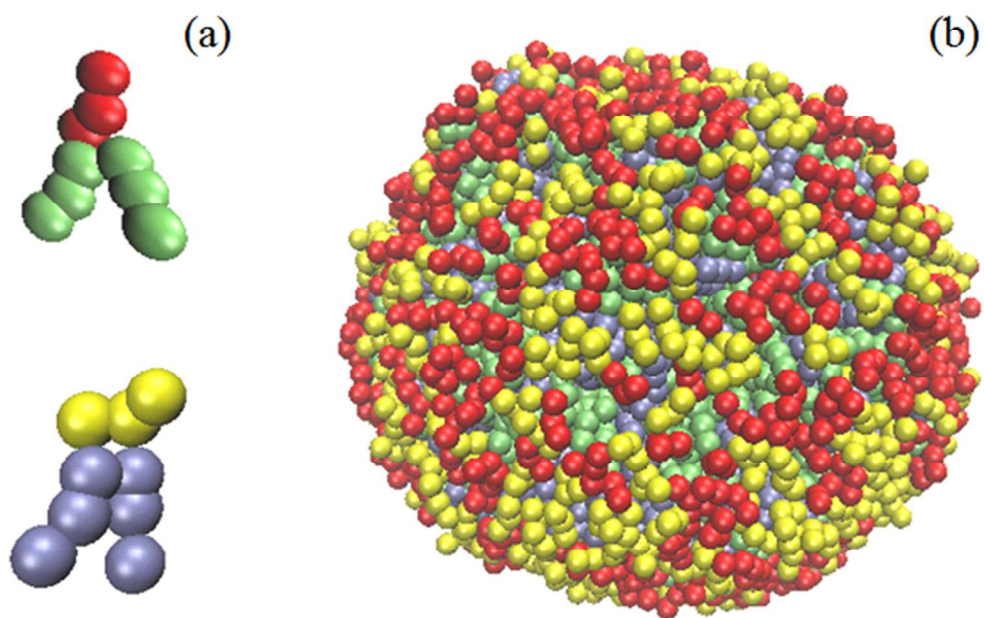


Figure 1

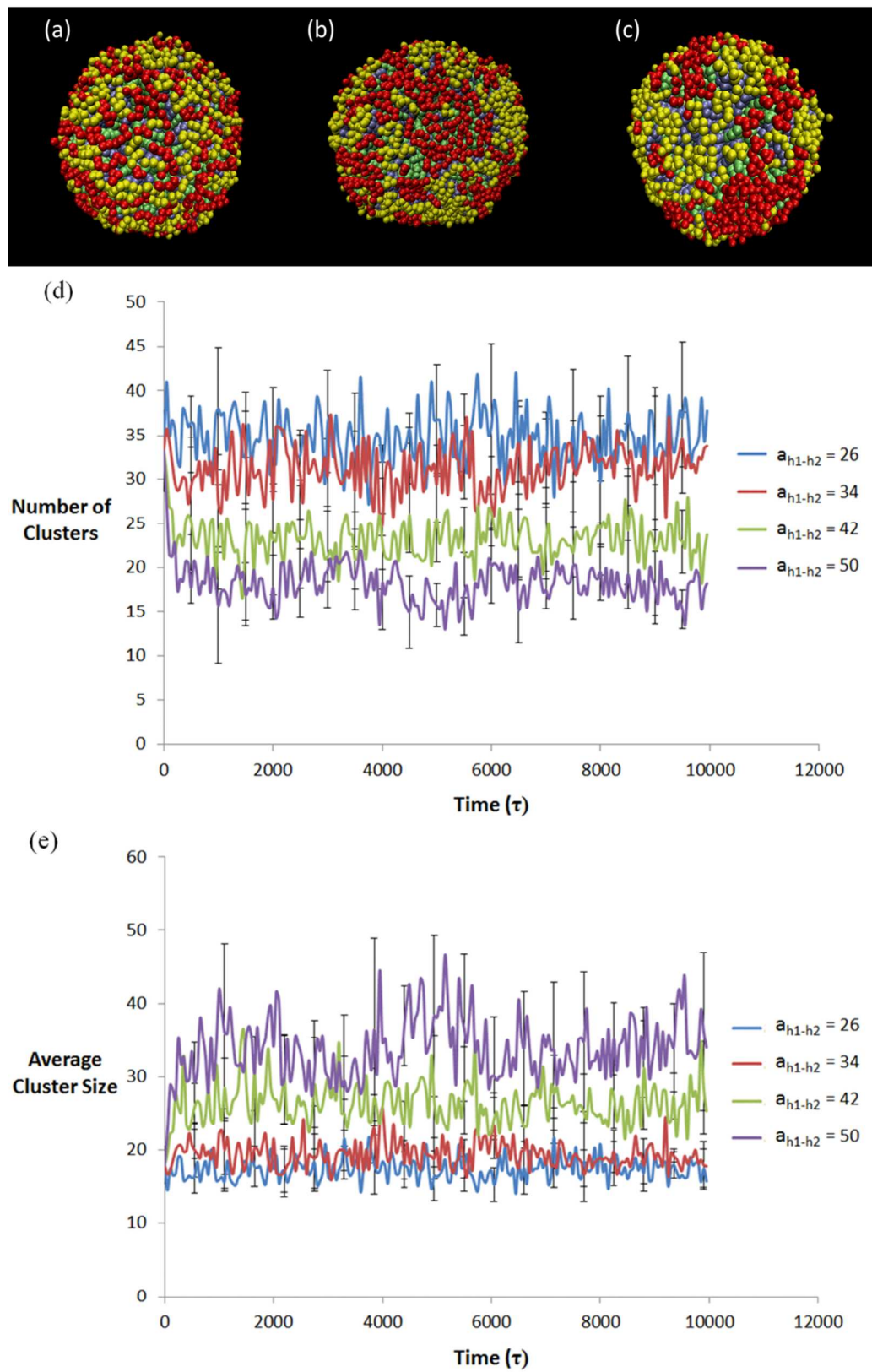


Figure 2

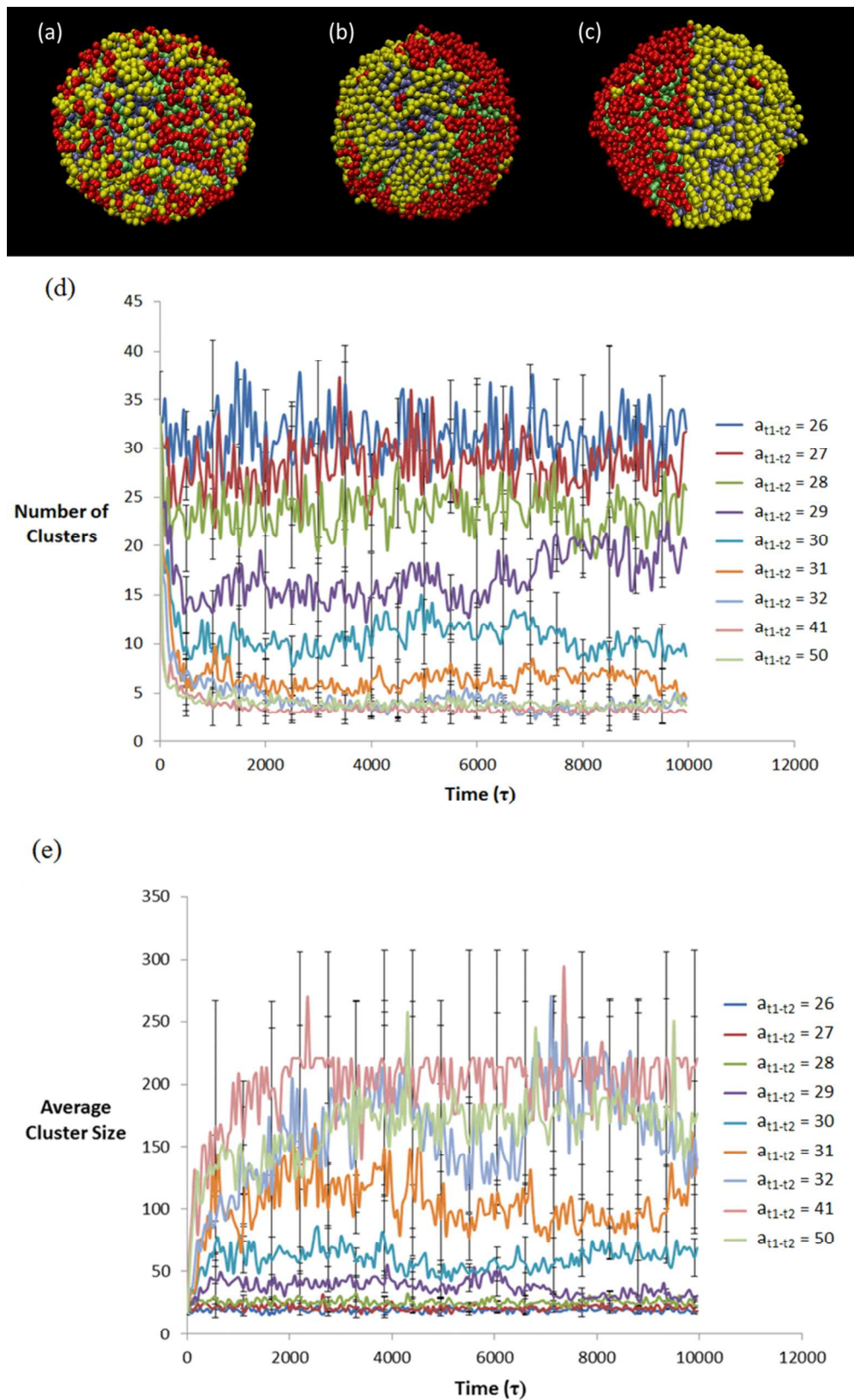


Figure 3

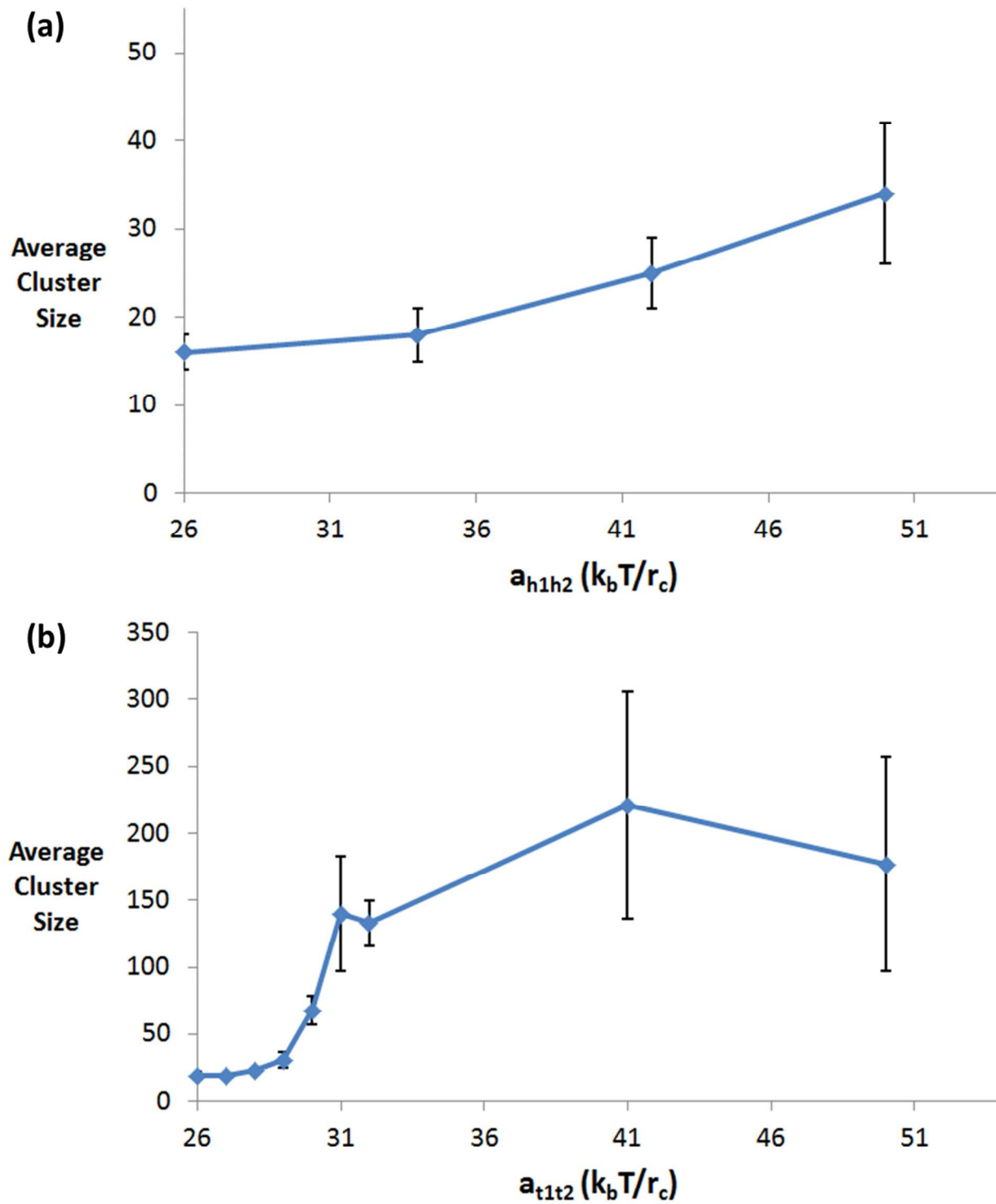


Figure 4

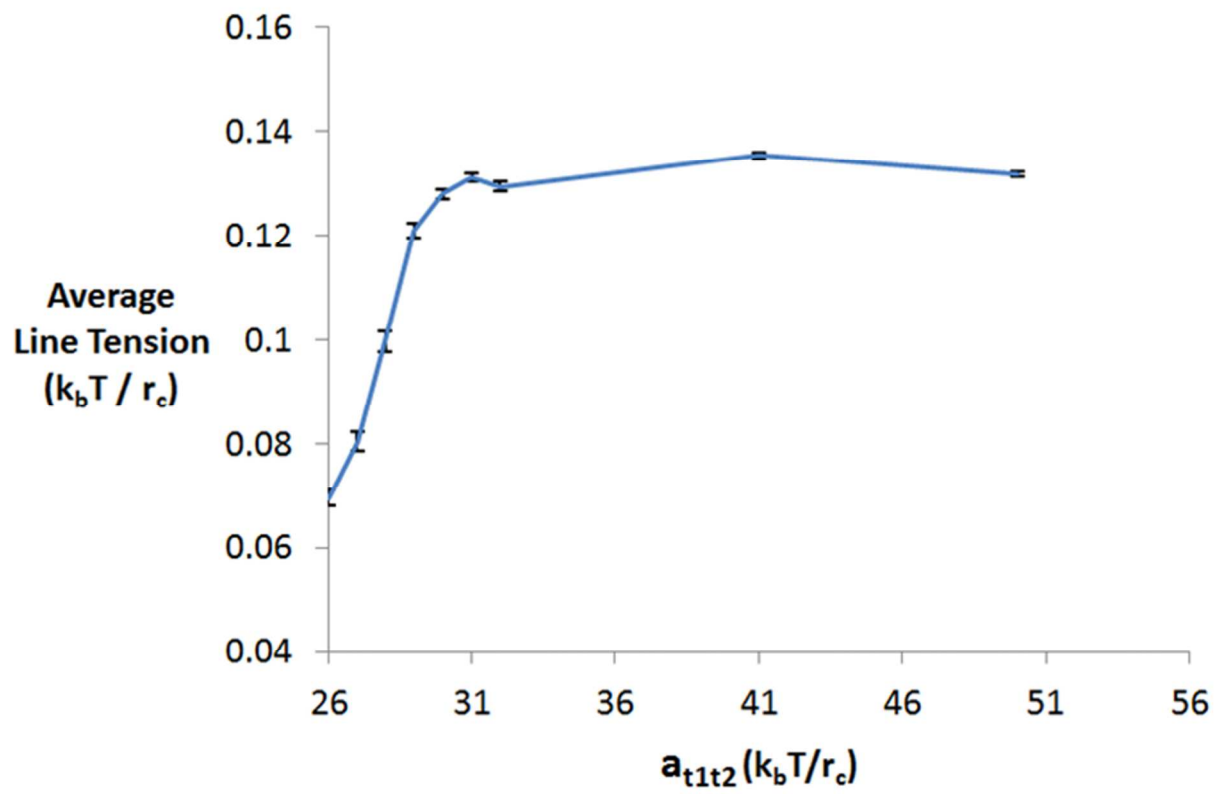


Figure 5

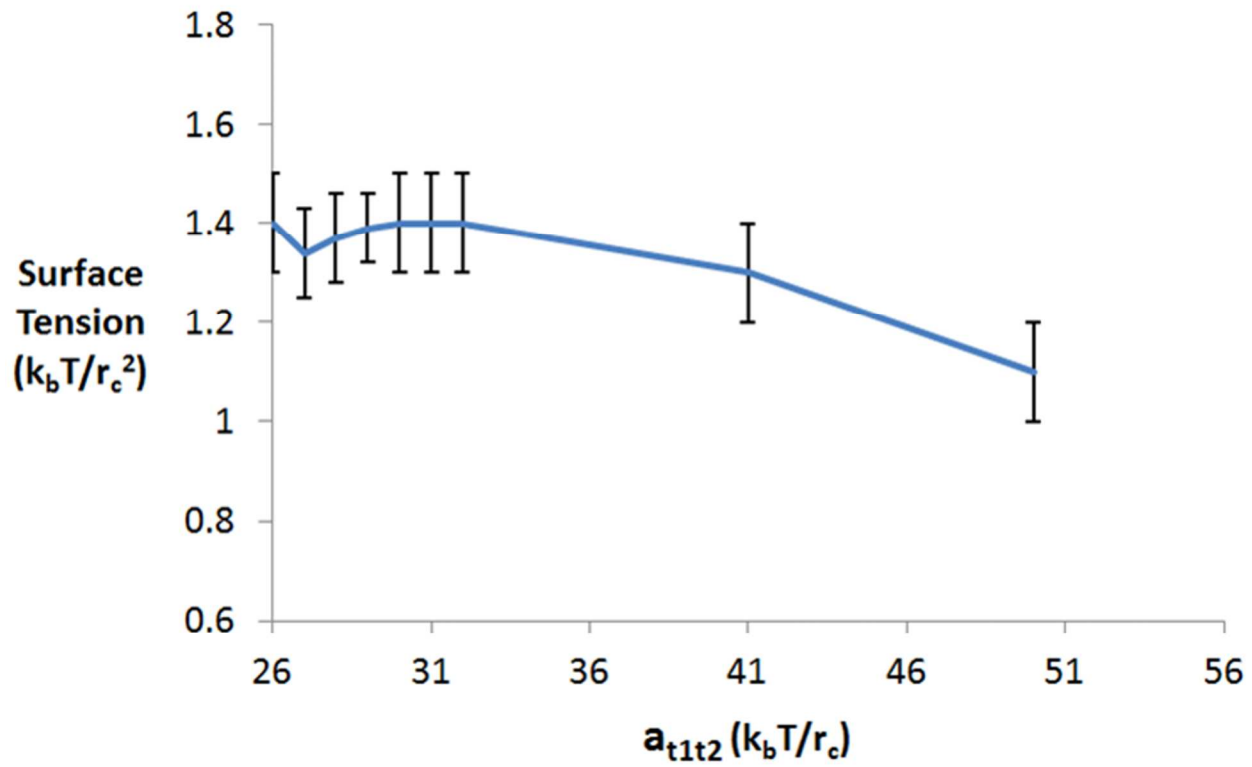


Figure 6

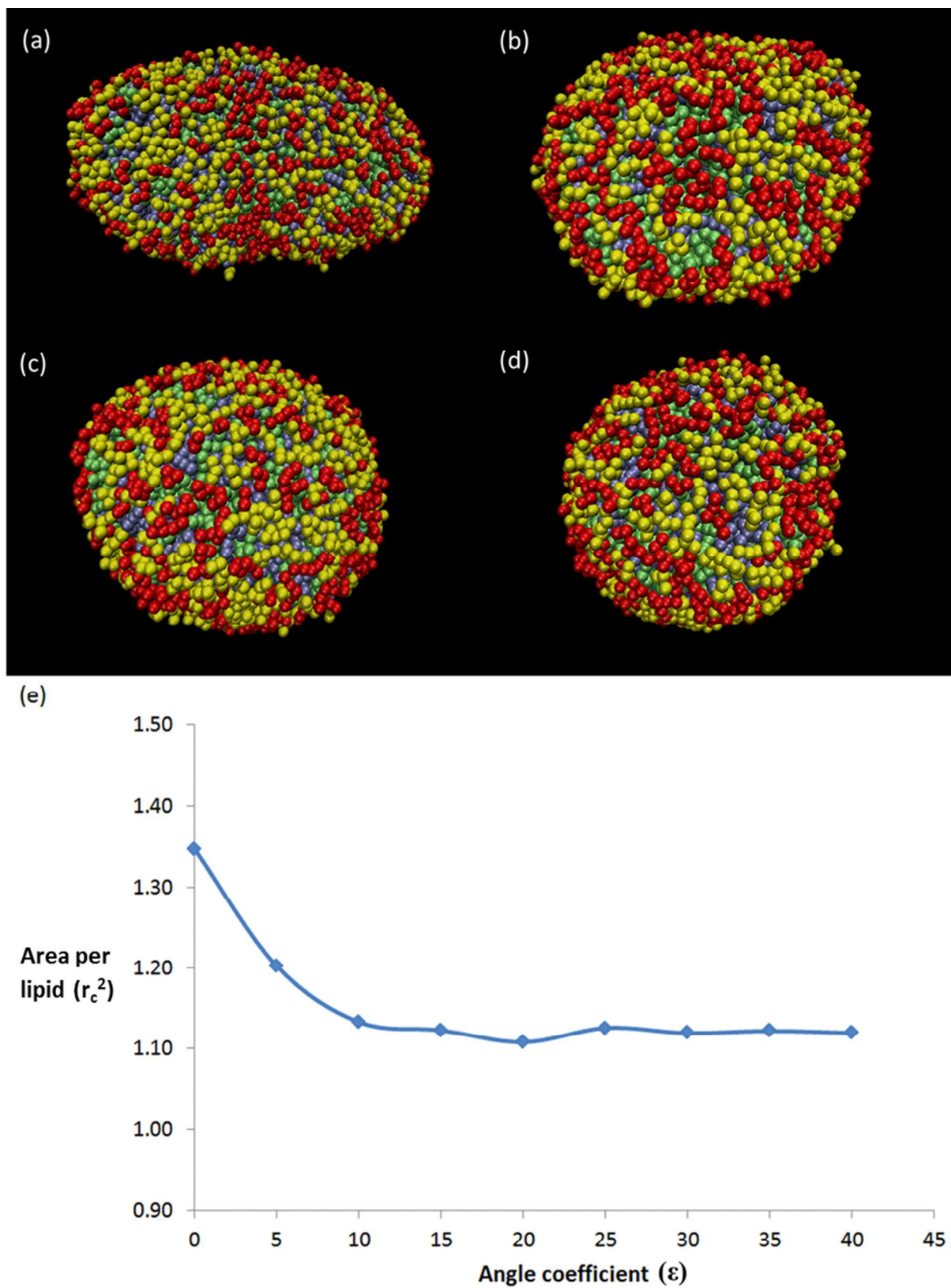


Figure 7

$a_{ij} (k_b T / r_c)$	Head 1	Tail 1	Head 2	Tail 2	Solvent
Head 1	25	100	—	100	25
Tail 1	100	25	100	—	100
Head 2	—	100	25	100	25
Tail 2	100	—	100	25	100
Solvent	25	100	25	100	25

Table 1

$a_{t_1-t_2}$ ($k_b T/r_c$)	α	β
31	-0.57	0.61
32	-0.54	0.55
41	-0.51	0.56
50	-0.53	0.52

Table 2

$a_{t_1-t_2}$ ($k_b T/r_c$)	Bilayer Thickness (r_c)	Area per lipid (r_c^2)
31	6.24±0.04	1.13±0.02
32	6.24±0.04	1.13±0.02
41	6.25±0.05	1.16±0.03
50	6.28±0.04	1.18±0.04

Table 3